

Multicomponent heterojunction of Au-Ag₂Se-Pb₃(PO₄)₂ for plasmonic-enhanced photoelectrochemical performance

HONGYUAN TANG^a, JURUI ZHENG^a, JIANPING LI^a, QIN XU^b, HONGCHENG PAN^{a,*}

^aGuangxi Key Laboratory of Electrochemistry and Magnetochemistry Functional Materials, College of Chemistry and Bioengineering, Guilin University of Technology, 12 Jiangan Road, Guilin 541004, P. R. China

^bCollege of Chemistry and Chemical Engineering, Yangzhou University, Yangzhou 225002, P. R. China

We present a simple method to construct Au-Ag₂Se-Pb₃(PO₄)₂ multicomponent heterojunction. Firstly, PbSe nanoparticles were electrodeposited onto indium-tin-oxide-coated glass electrodes. Subsequently, the resulting PbSe/ITO electrode was immersed into a solution containing Ag⁺, PO₄³⁻, and surfactant at 60 °C for 24 h to form Ag₂Se nanoparticles-decorated Pb₃(PO₄)₂ nanorods heterojunction. Finally, the electrode was immersed into a solution containing AuCl₄⁻ ions to spontaneously grow Au nanoparticles onto the heterojunction. The photocurrent of the Au-Ag₂Se-Pb₃(PO₄)₂/ITO photoelectrodes is about 200-fold larger than that of the Ag₂Se-Pb₃(PO₄)₂/ITO electrode. The mechanisms of the formation of the heterojunction and the enhancement of the photocurrent were discussed.

(Received February 12, 2017; accepted November 28, 2017)

Keyword: Heterojunction, Ag₂Se, Pb₃(PO₄)₂, Au, Photocurrent

1. Introduction

Semiconductor-based photocatalysts have attracted considerable interest for their potential applications in clean energy generation and environmental remediation [1-3]. However, the efficiency of semiconductor photocatalyst is limited by their fast rate of charge-carrier recombination and low visible-light absorption. This problem can be solved by modifying the electronic band structure for visible-light harvesting and separating photogenerated charge [2, 3]. Among alternative strategies for improving the photocatalytic efficiency, the formation of a semiconductor heterojunction by combining them with metal and/or other semiconductors has been one of the most effective methods [4, 5].

Some phosphate salts, such as Ag₃PO₄, BiPO₄, Cu₂(OH)PO₄, calcium phosphate, and cobalt phosphate (Co-Pi), have been demonstrated to be excellent photocatalysts [6-14]. Pb₃(PO₄)₂, a traditional ferroelastic material, however, exhibits a lower photocatalytic activity than its other phosphate counterparts. Recently, several efforts have been devoted to extend applications of Pb₃(PO₄)₂ to environmental remediation and catalysis for ethane oxydehydrogenation [15-17]. Singh et al. calculated electronic structure of Pb₃(PO₄)₂ and suggested a band gap of approximately 3.0 eV [18]. Due to its wide band gap, the photocatalytic activity of Pb₃(PO₄)₂ in visible light is very low. The photocatalytic activity may be improved by

constructing a semiconductor-semiconductor heterojunction or the semiconductor-metal heterojunction, or combining both to form a multicomponent heterojunction [2, 19-21].

Bulk Ag₂Se is a narrow band gap semiconductor with a band gap of 0.15 eV. The band gaps of nanostructured Ag₂Se can vary from 1.13 to 1.8 eV due to the quantum size effect [22-24]. By using the band gap value and Mulliken electronegativity, the valence band top (E_{CB}) of nanostructured Ag₂Se can be estimated as from 0.94 eV to 1.28 eV, which are lower than that of Pb₃(PO₄)₂ (3.19 eV) [25]. Therefore, the band structures of Ag₂Se and Pb₃(PO₄)₂ meet the requirements to form a heterojunction that may facilitate the transfer of charge carriers and retard the e^-h^+ recombination, resulting in improved photocatalytic performance. Another advantages of using Ag₂Se is that selenide may be favorable to form a semiconductor-metal (e.g. Au) heterojunction, which leads to charge separation that facilitates photocurrent generation [26, 27]. However, it is a great challenge to fabricate an Au-Ag₂Se-Pb₃(PO₄)₂ heterojunction. To the best of our knowledge, there are no reports on fabricating such a multicomponent heterojunction.

In this paper, we present a simple and facile method to construct Au-Ag₂Se-Pb₃(PO₄)₂ heterojunction. The first step in the procedure is to electrodeposit PbSe nanoparticles onto indium-tin-oxide-coated (ITO) glass electrodes. Subsequently, an one-step ion-exchange

strategy was applied to simultaneously form Ag₂Se nanoparticles-decorated Pb₃(PO₄)₂ nanorods heterojunction. Finally, Au nanoparticles were spontaneously grown onto the heterojunction. The morphology and structure of the Au-Ag₂Se-Pb₃(PO₄)₂ heterojunction were studied, and enhanced photocurrents of the heterojunction were observed. Furthermore, we propose mechanisms to explain the formation of the heterojunction and the enhanced photocurrent.

2. Experimental

2.1. Chemicals and materials

Pb(NO₃)₂, sodium dodecyl benzene sulfonate (SDBS), silver nitrate (AgNO₃), and HAuCl₄·4H₂O were purchased from Sinopharm (Shanghai, China). Acetic acid (CH₃COOH), sodium acetate trihydrate (CH₃COONa·3H₂O), Dibasic Sodium Phosphate (Na₂HPO₄·12H₂O), sodium sulfate (Na₂SO₄), and ethylenediaminetetraacetic acid disodium salt (EDTA) were purchased from Xilong chemical engineering (Shantou, China). Cetyltrimethylammonium chloride (CTAC) was obtained from Beijing chemical reagent (Beijing, China). Indium-tin-oxide-coated (ITO) glass electrodes (7 Ω/sq, 13×30×1.1 mm) were from Kaivo optoelectronic (Zhuhai, China). Other reagents were of analytical grade. Ultrapure water (resistivity>18 MΩ cm) was obtained from a WP-UP-IV-30 purification system (Woter, China) and used in the all experiments.

2.2. Electrodeposition of PbSe thin films onto ITO-coated glass substrates

The film electrodeposition was carried out using a three-electrode system consisting of an indium-doped tin oxide (ITO) covered glass as the working electrode, an Ag/AgCl as the reference electrode, and a Pt plate as the counter electrode. Cyclic voltammetry was carried out using a CHI660B electrochemical workstation (CH Instruments Inc., China). All potentials were measured against an Ag/AgCl reference. The ITO substrates were cleaned ultrasonically in acetone, ethanol, and then rinsed in ultrapure water. The electrodeposition of PbSe was performed by cycling the potential from 0 V and -1 V using a scan rate of 50 mV/s for 20 cycles in a solution containing 0.02 M Pb(NO₃)₂, 0.03M EDTA, 3mM SeO₂, and 0.46 M Na₂SO₄. The resulting dark brown film (hereafter referred as PbSe/ITO) was washed with ultrapure water, and dried in air at room temperature.

2.3. Conversion of PbSe/ITO into Ag₂Se-Pb₃(PO₄)₂/ITO nanoheterojunction thin films

The PbSe/ITO substrate was vertically immersed into a 10-mL solution containing 0.2 mM AgNO₃, 4 mM Na₂HPO₄, and 1% (w/w) SDBS at 60 °C for 24 h. The resulting slide (hereafter referred as Ag₂Se-Pb₃(PO₄)₂/ITO) was washed with ultrapure water, and dried in air at room temperature.

2.4. Spontaneous growth of Au nanoparticles onto Ag₂Se-Pb₃(PO₄)₂/ITO slide

To a 20-mL beaker was sequentially added with 5 mL of ultrapure water, 300 μL of 0.2 M acetic acid buffer solution (NaAc-HAc, pH=6.0), 25 μL of HAuCl₄ (1%, w/w), and 80 μL of 0.2 M CTAC. The Ag₂S-Pb₃(PO₄)₂/ITO slide was immersed in the above solution at 60 °C for 3 h. After the growth of Au nanoparticles, the slide was washed with ultrapure water, dried in air, and hereafter referred as Au-Ag₂Se-Pb₃(PO₄)₂/ITO.

2.5. Characterization and electrochemical measurements

The surface morphology and surface element analysis were obtained with a Hitachi S-4800 scanning electron microscope (SEM) equipped with an energy dispersive X-ray (EDX) detector. X-ray Power diffraction (XRD) measurements were carried out on an X-ray diffractometer (X'pert PRO, Philips, Eindhoven, Netherlands). Photoelectrochemical measurements were performed with a homemade photoelectrochemical system. A 300 W Xenon lamp was used as the irradiation source. Photocurrent was measured on a CHI 660B electrochemical workstation. An Au-Ag₂Se-Pb₃(PO₄)₂/ITO electrode with an area of 1 cm² was employed as the working electrode. A Pt wire was used as the counter electrode, and a saturated Ag/AgCl electrode was used as the reference electrode. All photocurrent measurements were performed at a constant potential of 0 V (vs saturated Ag/AgCl) in a 0.2 M phosphate buffer solution (PBS, pH =6.8).

3. Results and discussion

3.1. Electrodeposition of PbSe thin films onto ITO substrates

Fig. 1a depicts a typical cyclic voltammogram (the first cycle) for the electrodeposition of PbSe onto ITO

substrate. The CV was initiated at 0.0 V, scanned in the negative direction and reversed at -1.0 V in the positive direction. The first reduction wave observed at -0.29 V is contributed to the reduction of Se(IV) to Se(0) [28]. The rapid increase in current observed at -0.72 V, is assigned to the commencement of the electrodeposition of PbSe at the ITO cathode. The current increased sharply to the potential at -0.89 V and subsequently decreased. The potential scan was reversed at -1.0 V and the current decreased and subsequently formed a “nucleation loop” between the cathodic and anodic branches (from -0.619 to -0.756 V), indicating the formation of PbSe nuclei on ITO substrate. In the reversed scan the first oxidation peak is observed at -0.31 V, which correspond to the oxidation of elemental lead.

The surface morphology of electrodeposited PbSe thin films were characterized by SEM (Fig. 1b). The PbSe film is composed of small crystallites with diameters of several nanometers, most of which have coalesced to form cauliflower-shaped nanostructures (several hundred nanometers in size). The XRD results (Fig. 1c) support the formation of PbSe on the surface of the ITO slides.

3.2. Conversion of PbSe/ITO into Ag₂Se-Pb₃(PO₄)₂/ITO heterojunction thin films

If the PbSe/ITO slides are immersed in a Na₂HPO₄ solution, PbSe converts to Pb₃(PO₄)₂ because the solubility product of Pb₃(PO₄)₂ ($K_{sp}=4\times 10^{-45}$) is lower than that of the PbSe ($K_{sp}=10^{-38}$). However, this process proceeds very slowly that no significant conversion occurs before 4 d. The addition of an appropriate amount of AgNO₃ significantly accelerates the process. This may be attributed to the formation of insoluble Ag₂Se, whose solubility product ($K_{sp}=2\times 10^{-64}$) is much lower than that of PbSe and Pb₃(PO₄)₂. Ag⁺ ions can be adsorbed on PbSe crystal surface to form Ag₂Se and release Pb²⁺ ions into the solution. Because of the simultaneous presence of Pb²⁺ and PO₄³⁻, Pb₃(PO₄)₂ is formed and deposited on the ITO substrate surface. The SEM image (Fig. 1b) shows clearly that PbSe particles disappeared after immersion in a solution containing AgNO₃, Na₂HPO₄ and 1% SDBS 60 °C for 24 hours. However, it can be seen that a number of nanorods with diameters of 60-100 nm and lengths of 1-2 μm were formed on the surface of the ITO substrate. The morphology of the nanorods are almost the same as that of Pb₃(PO₄)₂ grown from a Na₂HPO₄ solution without AgNO₃, except that the nanorods are decorated with some 20-30 nm-sized nanoparticles. From the SEM images, we can conclude that the nanorods are Pb₃(PO₄)₂ and the nanoparticles are Ag₂Se. This deduction was also confirmed by XRD analysis (Fig. 2c).

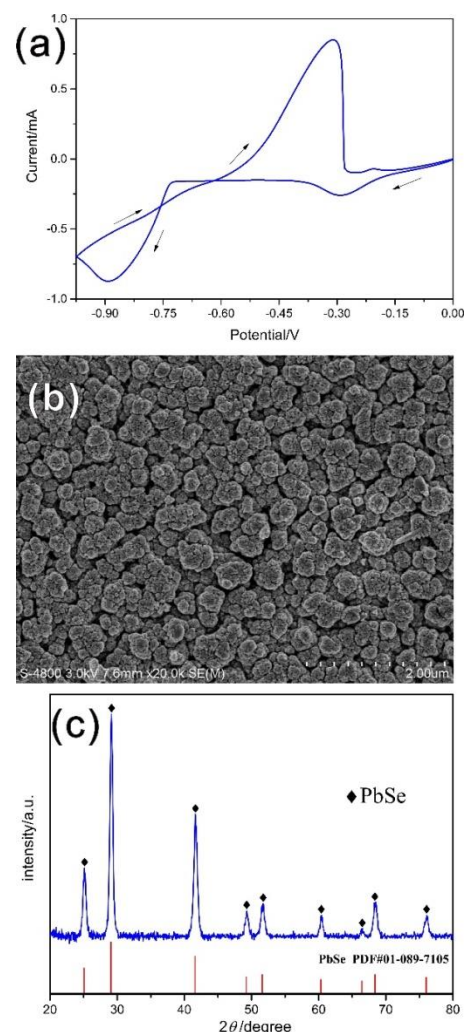


Fig. 1. (a) the first cycle of cyclic voltammograms for PbSe electrodeposition, (b) SEM image, and (c) XRD of the PbSe/ITO slide

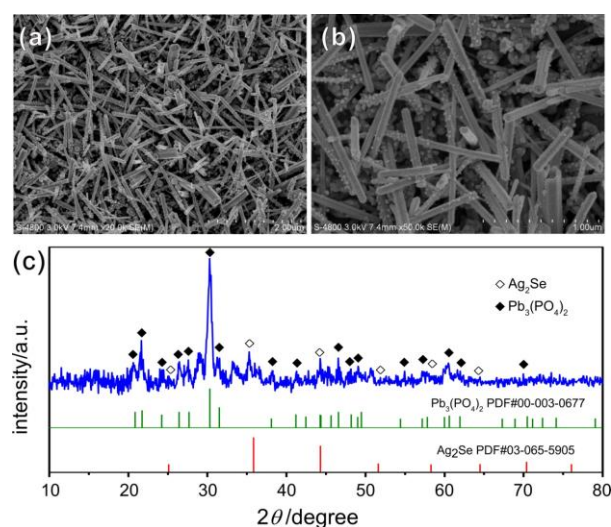


Fig. 2. (a) low and (b) high magnification SEM images, and (c) XRD of Ag₂Se-Pb₃(PO₄)₂/ITO

3.3. Growth of Au nanoparticles onto the $\text{Ag}_2\text{Se-Pb}_3(\text{PO}_4)_2/\text{ITO}$ slides

After the $\text{Ag}_2\text{Se-Pb}_3(\text{PO}_4)_2/\text{ITO}$ slides were immersed in the Au growth solution containing HAuCl_4 , NaAc-HAc , and CTAC for several hours, the films became darker with a brown-red coloration with the increase of growth time. This color change may be due to the growth of gold. The XRD (Fig. 3a) analysis confirms the presence of metallic gold in the slides. Three diffraction peaks at 2θ values of 38.22° , 44.23° , and 64.23° , corresponding to (111), (200), and (220) crystalline planes, respectively, suggest the formation of the face-centered cubic crystalline gold (PDF#01-089-3697). This result is in good agreement with energy dispersive X-ray (EDX) analysis (Fig. 3b).

Fig. 3c depicts a typical SEM micrograph of the Au nanoparticles for a deposition time of 1 h. A few large nanoparticles with diameters of 100-200 nm appeared after the growth of Au for 1 h. Further increasing the growth time to 3 h, more and larger particles with diameter of 100-300 nm were observed and the nanorods were coated with homogeneous coating layers (Fig. 3). According to the results of XRD EDX, and SEM, we conclude that Au nanoparticles were grown on the surface of $\text{Ag}_2\text{Se-Pb}_3(\text{PO}_4)_2/\text{ITO}$.

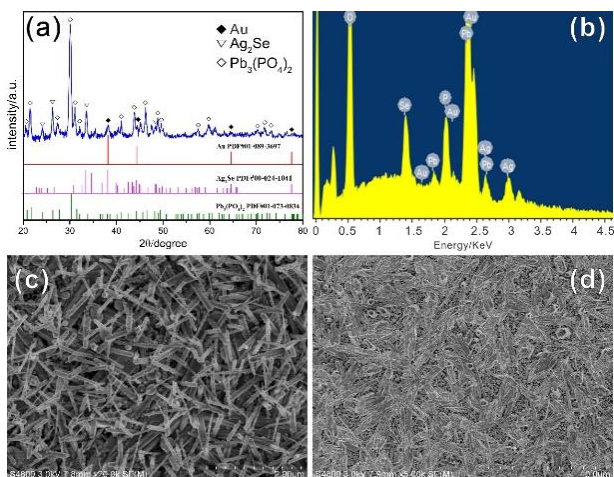


Fig. 3. (a) XRD and (b) EDX of $\text{Au-Ag}_2\text{Se-Pb}_3(\text{PO}_4)_2/\text{ITO}$; SEM images of $\text{Au-Ag}_2\text{Se-Pb}_3(\text{PO}_4)_2/\text{ITO}$ for the growth time of (c) 1 h and (d) 3 h

On the basis of our findings, we propose a possible mechanism for the spontaneous growth of Au nanoparticles onto the $\text{Ag}_2\text{Se-Pb}_3(\text{PO}_4)_2$. The formation of Au nanoparticles may undergo adsorption and redox processes. It is well known that Au(III) ions are easily adsorbed onto the surface of sulfides via the strong Au-S bond. Recent studies show that the Au-Se bond is stronger than the corresponding Au-S bond by approximately 0.4

eV [29]. Therefore, we believe that AuCl_4^- ions can be adsorbed onto Ag_2Se surface. The AuCl_4^- ions on the surface of Ag_2Se can be immediately reduced to Au by selenide, because the standard reduction potential of $\text{AuCl}_4^-/\text{Au}$ redox pair (1.002 V vs. the standard hydrogen electrode (SHE)) is higher than that of the Se/Se^{2-} (-0.924 V vs. SHE). The elemental gold should be mainly confined to the vicinity of the Ag_2Se surface. Once the concentration of Au atoms has reached a critical value, they will nucleate and grow into small clusters, and eventually form Au nanoparticles.

3.4. Photoelectrochemical properties of the $\text{Au-Ag}_2\text{Se-Pb}_3(\text{PO}_4)_2/\text{ITO}$

For comparison, we investigated the PEC properties of three photoelectrodes: PbSe/ITO , $\text{Ag}_2\text{Se-Pb}_3(\text{PO}_4)_2/\text{ITO}$, and $\text{Au-Ag}_2\text{Se-Pb}_3(\text{PO}_4)_2/\text{ITO}$ photoelectrodes. As shown in Fig. 4a, the PbSe/ITO photoelectrode displayed a very low photocurrent ($0.1 \mu\text{A}/\text{cm}^2$) under illumination. After the formation of $\text{Ag}_2\text{Se-Pb}_3(\text{PO}_4)_2$ heterojunction, the photocurrent was slightly increased to $0.14 \mu\text{A}/\text{cm}^2$. A significant enhancement of the photocurrent was observed on the $\text{Au-Ag}_2\text{Se-Pb}_3(\text{PO}_4)_2/\text{ITO}$. Upon irradiation, the $\text{Au-Ag}_2\text{Se-Pb}_3(\text{PO}_4)_2/\text{ITO}$ prepared by grown Au nanoparticles for 1 h produced a pronounced photocurrent spike of $31 \mu\text{A}/\text{cm}^2$, which is approximately 200 times higher than that of the $\text{Ag}_2\text{Se-Pb}_3(\text{PO}_4)_2/\text{ITO}$ electrode. This photocurrent spike can be attributed to the generation and separation of the electron/hole pairs [30]. When the light was off, the separated electron/hole pairs immediately recombined, resulting in a sharp drop in the photocurrent. No decay tail was observed, indicating the highly efficient charge transport. Once the light was switched on again, the photocurrent reverted to the original value. The photocurrent kept almost constant and instantaneous changes upon illumination on/off cycles.

The enhancement of the photocurrent can be attributed to the formation of intense electric fields at the Au nanoparticle surface, which increase the rate of formation of electron/hole (e^-/h^+) pairs at the nearby $\text{Ag}_2\text{Se-Pb}_3(\text{PO}_4)_2$ heterojunction surface. The advantage of the formation of e^-/h^+ pairs near the $\text{Ag}_2\text{Se-Pb}_3(\text{PO}_4)_2$ heterojunction surface is that these charge carriers are readily separated from each other and easily migrate to the surface, where they can perform photocatalytic transformations.

We investigated the photoelectrochemical performance of the $\text{Au-Ag}_2\text{Se-Pb}_3(\text{PO}_4)_2/\text{ITO}$ electrodes with different Au-grown time under illumination. As seen in Fig. 4b, the maximum photocurrent is observed at a growth times of 1 h. A tendency toward decreased photocurrents was shown with increasing the growth time of Au. This photocurrent decrement may due to the quenching effect by more coating of Au and the dense packing of Au nanoparticles, which is similar to those

previously reported [31].

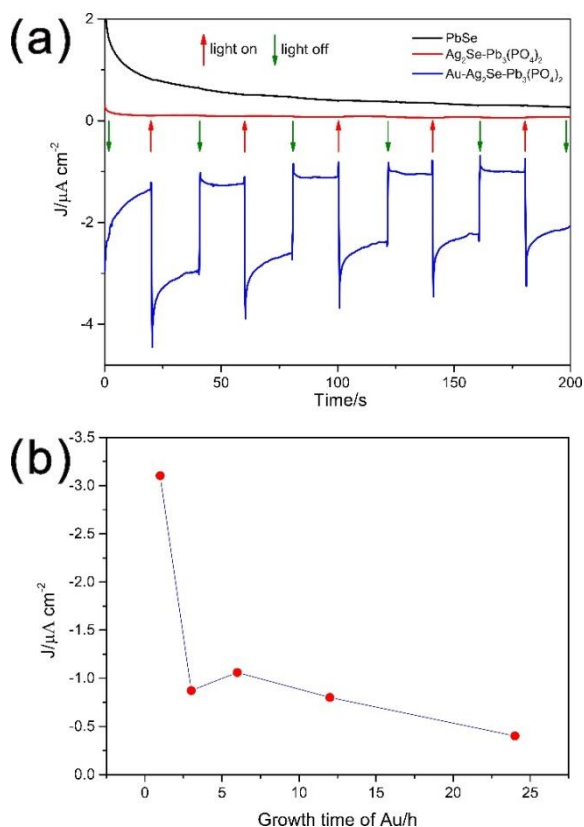


Fig. 4. (a) The photocurrents of the PbSe/ITO, Ag₂Se-Pb₃(PO₄)₂/ITO, and Au-Ag₂Se-Pb₃(PO₄)₂/ITO photoelectrodes; (b) dependence of the growth times of Au on the photocurrents

4. Conclusions

We have presented a simple method for fabricating Au-Ag₂Se-Pb₃(PO₄)₂ multicomponent heterojunction and investigated the photoelectrochemical properties of the heterojunction. Our method has two main advantages: 1) through using an one-step ion-exchange strategy, Ag₂Se nanoparticles and Pb₃(PO₄)₂ nanorods were simultaneously synthesized and the heterojunction was *in situ* formed by decorated Ag₂Se nanoparticles onto Pb₃(PO₄)₂ nanorods; 2) Au nanoparticles were spontaneously grown onto the surface of Ag₂Se-Pb₃(PO₄)₂ heterojunction, without adding reducing agents. After growth of Au nanoparticles, the photocurrent of the Au-Ag₂Se-Pb₃(PO₄)₂/ITO photoelectrode produced a maximum enhancement up to 200-fold compare with that of the Ag₂Se-Pb₃(PO₄)₂/ITO electrode. The enhancement of the photocurrent can be explained by the formation of intense electric fields at the Au nanoparticle surface, which increase the rate of formation of e⁻/h⁺ pairs at the nearby Ag₂Se-Pb₃(PO₄)₂ heterojunction surface.

Acknowledgments

This work was supported by National Natural Science Foundation of China (20905016, 21265005), Guangxi Natural Science Foundation (2013GXNSFBB053009), the project of high level innovation team and outstanding scholar in Guangxi colleges and universities, Guangxi colleges and universities key laboratory of food safety and detection, collaborative innovation center for water pollution control and water safety in karst area, and Guangxi key laboratory of environmental pollution control theory and technology.

References

- [1] X. Chen, S. Shen, L. Guo, S. S. Mao, Chem. Rev. **110**(11), 6503 (2010).
- [2] H. Wang, L. Zhang, Z. Chen, J. Hu, S. Li, Z. Wang, J. Liu, X. Wang, Chem. Soc. Rev. **43**(15), 5234 (2014).
- [3] R. Marschall, Adv. Funct. Mater. **24**(17), 2421 (2014).
- [4] H. Huang, S. Wang, N. Tian, Y. Zhang, RSC Adv. **4**(11), 5561 (2014).
- [5] W. Shi, F. Guo, J. Chen, G. Che, X. Lin, J. Alloy. Compd. **612**, 143 (2014).
- [6] Z. Li, Y. Dai, X. Ma, Y. Zhu, B. Huang, Phys. Chem. Chem. Phys. **16**(7), 3267 (2014).
- [7] C. Piccirillo, C. W. Dunnill, R. C. Pullar, D. M. Tobaldi, J. A. Labrincha, I. P. Parkin, M. M. Pintado, P. M. L. Castro, J. Mater. Chem. A **1**(21), 6452 (2013).
- [8] Y. Wang, Y. Wang, R. Jiang, R. Xu, Ind. Eng. Chem. Res. **51**(30), 9945 (2012).
- [9] D. J. Martin, G. Liu, S. J. Moniz, Y. Bi, A. M. Beale, J. Ye, J. Tang, Chem. Soc. Rev. **44**(21), 7808 (2015).
- [10] Y. Bi, S. Ouyang, N. Umezawa, J. Cao, J. Ye, J. Am. Chem. Soc. **133**(17), 6490 (2011).
- [11] W. Wang, B. Cheng, J. Yu, G. Liu, W. Fan, Chem. Asian J. **7**(8), 1902 (2012).
- [12] G.-F. Huang, Z.-L. Ma, W.-Q. Huang, Y. Tian, C. Jiao, Z.-M. Yang, Z. Wan, A. Pan, J. Nanomater. **2013**, 1 (2013).
- [13] C. S. Pan, Y. F. Zhu, Environ. Sci. Technol. **44**(14), 5570 (2010).
- [14] G. Wang, B. Huang, X. Ma, Z. Wang, X. Qin, X. Zhang, Y. Dai, M.-H. Whangbo, Angew. Chem. Int. Ed., **52**(18), 4810 (2013).
- [15] M. Chrysochoou, D. Dermatas, D.G. Grubb, J. Hazard. Mater. **144**(1-2), 1 (2007).
- [16] X. Cao, L. Q. Ma, S. P. Singh, Q. Zhou, Environ. Pollut. **152**(1), 184 (2008).
- [17] S. Zhong, F. Gao, S. Jiang, Chinese J. Catal. **21**(2), 147 (2000).
- [18] D. J. Singh, G. E. Jellison, L. A. Boatner, Phys. Rev. B **74**(15), 155126 (2006).
- [19] R. Jiang, B. Li, C. Fang, J. Wang, Adv. Mater. **26**(31), 5274 (2014).
- [20] A. Dawson, P. V. Kamat, J. Phys. Chem. B **105**(5),

- 960 (2001).
- [21] W. Hou, S.B. Cronin, *Adv. Funct. Mater.* **23**(13), 1612 (2013).
- [22] S.-Y. Zhang, Chun-Xia Fang, W. Wei, B.-K. Jin, Y.-P. Tian, Y.-H. Shen, Jia-Xiang Yang, H.-W. Gao, *J. Phys. Chem. C* **111**(11), 4168 (2007).
- [23] B. Pejova, M. Najdoski, I. Grozdanov, S. K. Dey, *Mater. Lett.* **43**, 629 (2000).
- [24] C. N. Zhu, P. Jiang, Z. L. Zhang, D. L. Zhu, Z. Q. Tian, D. W. Pang, *ACS Appl. Mater. Inter.* **5**(4), 1186 (2013).
- [25] J. J. Liu, X. L. Fu, S. F. Chen, Y. F. Zhu, *Appl. Phys. Lett.* **99**, 19193 (2000).
- [26] J.-S. Lee, E. V. Shevchenko, D. V. Talapin, *J. Am. Chem. Soc.* **130**(30), 9673 (2008).
- [27] L. Sheeney-Haj-Idia, S. Pogorelova, Y. Gofer, I. Willner, *Adv. Funct. Mater.* **14**(5), 416 (2004).
- [28] H. Saloniemi, T. Kanninen, M. Ritala, M. Leskela, R. Lappalainen, *J. Mater. Chem.* **8**(3), 651 (1998).
- [29] S. M. A. G. G. Wendin, *Nanotechnology* **14**(8), 849 (2003).
- [30] Y. Dai, Y. Sun, J. Yao, D. Ling, Y. Wang, H. Long, X. Wang, B. Lin, T. H. Zeng, Y. Sun, *J. Mater. Chem. A* **2**(4), 1060 (2014).
- [31] Y. Takahashi, S. Taura, T. Akiyama, S. Yamada, *Langmuir* **28**(24), 9155 (2012).

*Corresponding author: hcpan@163.com